Title: Punishment-Predictive Cues Guide Avoidance through Potentiation of Hypothalamus-to-Habenula Synapses.

Authors: Trusel M, Nuno-Perez A, Lecca S, Harada H, Lalive AL, Congiu M, Takemoto K, Takahashi T, Ferraguti F, Mameli M

Journal: Neuron

Year: 2019 Apr 3

Issue: 102

Volume: 1

Pages: 120-127.e4

DOI: 10.1016/j.neuron.2019.01.025

Punishment-predictive cues guide avoidance through potentiation of hypothalamus-to-habenula synapses.

Massimo Trusel[1], Alvaro Nuno-Perez[1], Salvatore Lecca[1], Harumi Harada[3], Arnaud L. Lalive[1], Mauro Congiu[1], Kiwamu Takemoto[4], Takuya Takahashi[4], Francesco Ferraguti[3], and Manuel Mameli[1,2*]

[1] The Department of Fundamental Neuroscience, The University of Lausanne 1005 Lausanne, Switzerland.

[2] Inserm, UMR-S 839, 75005 Paris, France.

[3] Department of Pharmacology, Medical University of Innsbruck, A-6020, Innsbruck, Austria.

[4] Department of Physiology, Graduate School of Medicine Yokohama City University, 236-0004 Yokohama, Japan.

*Lead contact: Manuel Mameli, PhD

The Department of Fundamental Neuroscience, The University of Lausanne 1005 Lausanne, Switzerland.

Email manuel.mameli@unil.ch

Summary

Throughout life, individuals learn to predict a punishment via its association with sensory stimuli. This process ultimately prompts goal-directed actions to prevent the danger, a behavior defined as avoidance. Neurons in the lateral habenula (LHb) respond to aversive events, as well as to environmental cues predicting them, supporting LHb contribution to cue-punishment association. However, whether synaptic adaptations at discrete habenular circuits underlie such associative learning to instruct avoidance remains elusive. Here, we find that, in mice, contingent association of an auditory cue (tone) with a punishment (foot-shock) progressively causes cue-driven LHb neuronal excitation during avoidance learning. This process is concomitant with the strengthening of LHb AMPAR-mediated neurotransmission. Such phenomenon occludes long-term potentiation and occurs specifically at hypothalamus-to-habenula synapses. Silencing hypothalamic-to-habenula inputs or optically inactivating postsynaptic AMPARs within the LHb disrupts avoidance learning. Altogether, synaptic strengthening at a discrete habenular circuit transforms neutral stimuli into salient punishment-predictive cues to guide avoidance.

Introduction

The sound of a fire alarm guides a rapid action to immediately ensure safety. This is an instance where associating environmental cues to aversive events grants individuals to predict and avoid threats, a primary strategy for survival. Neurons in the lateral habenula (LHb) are instrumental in processing aversive events, and guide innate escape behaviors. Unexpected punishments or disappointment phasically excite LHb neurons (Lecca et al., 2017; Matsumoto and Hikosaka, 2007; Wang et al., 2017). Importantly, after conditioning, punishment-predictive external cues are also efficient in driving LHb neuronal excitation (Matsumoto and Hikosaka, 2007). This suggests that the LHb may support cue-punishment learning. Such process is instrumental for adaptive behavioral strategies, including avoidance, a cardinal mechanism allowing individuals to prevent the predicted punishment (LeDoux et al., 2017).

Glutamatergic inputs from brain structures including the lateral hypothalamus (LH), the medial ventral tegmental area (mVTA), and the entopeduncular nucleus of the basal ganglia (EPN) increase LHb neuronal activity and guide aversive behaviors (Root et al., 2014; Stamatakis et al., 2016; Shabel et al., 2012). Importantly, such excitatory synapses can undergo activity-dependent synaptic plasticity (Valentinova and Mameli, 2016). Moreover, in pathological conditions, pre- and postsynaptic modifications of glutamatergic neurotransmission alter LHb neuronal output, and ultimately underlie depressive-like states (Lecca et al., 2016; Li et al., 2011; Meye et al., 2015). Altogether, this evidence supports the notion that synaptic plasticity at discrete inputs onto LHb synapses tunes LHb neurons firing and is causal for specific behavioral outcomes.

Long-term potentiation (LTP) of excitatory transmission is crucial for learning processes and enables neuronal networks to represent a memory (Nabavi et al., 2014). Yet, whether synaptic adaptations within habenular circuits represent a cellular substrate for associative learning occurring during avoidance remains poorly understood.

Here we examined whether cue-punishment associations, and the subsequent cue-driven avoidance *i.* engage LHb neuronal dynamics and *ii.* require pathway-specific synaptic plasticity.

Results

Punishment-predictive cues excite LHb neurons during avoidance learning

Aversive events or their predictors lead to a time-locked phasic excitation of LHb neurons (Matsumoto and Hikosaka, 2007). Here, we examined the progression of LHb neuronal dynamics throughout cue-punishment association and avoidance learning.

To model cue-punishment associative learning and subsequent cue-guided avoidance we employed a Two-Way Active Avoidance task (LeDoux et al., 2017). During 5 sessions (1 session/day; 30 trials/session), mice experienced a tone (CS, 10 sec) followed by a foot-shock (US). Foot-shock delivery would stop if mice crossed compartments (shuttles; Figure S1A). We examined avoidance learning by computing goal-directed shuttles during the CS. Mice progressively improve their shuttling performance thereby preventing shock occurrence (Learner group, L, Figure 1A). In contrast, control mice received similar amount of foot-shocks and tones (compared to L-mice), but CS and US were never contingent (Control group, C, Figure 1A).

To examine LHb neurons' activity during avoidance learning we employed photometric analysis of calcium-mediated fluorescent transients – used as a proxy for neuronal activity (Lecca et al., 2017). We virally expressed the fluorescent Ca^{2+} sensor GCaMP6f unilaterally in the LHb and implanted a multimodal fiber optic above the injection site to collect the emitted photons (Figure 1B and Figure S1B). Post-hoc analysis indicated that ~ 69% (2596/3729 neurons, 4 mice) of the LHb neuronal population expressed GCaMP6f and was glutamatergic (i.e. EAAC1+; Figure S1C and Figure S1D).

During the first training session, calcium fluorescent transients were time-locked to foot-shock delivery, with minimal transients evoked during CS presentation (Figure 1A and Figure 1B). During subsequent training days, while cue-punishment association and cue-driven shuttles progressed,

fluorescent transients were typically observed in response to both foot-shock and CS onset (Day 3; Figure 1B, Figure 1C and Figure S1E). The CS-driven phasic fluorescent responses, measured at the peak, gradually developed over the sessions to become, at day 5, significantly larger than day 1 (Figure 1C). CS-driven fluorescent transients were learning-driven and GCamp6f-mediated, as they were absent across the five sessions in control mice and GFP-only expressing learner animals (Figure S1E and Figure S1F). In contrast, the amplitude of US-driven transients remained comparable across training sessions supporting the stability over time of the photometric signal (Figure S1E, Figure S1G–I). Consistently, the ratio $CS_{photons}/US_{photons}$ at each session from individual learner mice correlated with the number of shuttle events during the CS (Figure 1D). Finally, single–unit recordings in awake mice corroborated that CS-driven LHb neurons excitation occurs in learner but not control mice (Figure S1J). Altogether, these data indicate that the transition from neutral to punishment-valued cues during avoidance learning associates with cue-evoked LHb neuronal excitation.

Avoidance learning and synaptic potentiation in the LHb.

Potentiation of excitatory synapses represents a neurobiological substrate underlying the association between cues and salient experiences. Accordingly, LTP may support the emergence of cue-valued excitation of midbrain dopamine neurons during reward prediction learning (Stuber et al., 2008).

We therefore tested the prediction that synaptic strengthening of excitatory transmission onto LHb neurons represents a core mechanism for cue-driven avoidance learning. To examine excitatory synaptic transmission onto LHb neurons along the progression of avoidance learning, we performed *ex-vivo* patch clamp experiments in LHb-containing acute slices from control and learner mice. Evoked excitatory postsynaptic currents (EPSCs) were recorded at different timings during the training – ~1 hour after session one (I), and 24 hours after session one (II), two (III), three (IV) and four (V) (Figure 2A). Bath application of the NMDAR antagonist D-2-amino-5-phosphonopentanoate (AP5) and digital subtraction allowed the isolation of synaptically-evoked AMPA- and NMDA-mediated currents (+40 mV; Figure 2A). This permitted

computing the AMPAR/NMDAR ratio, a validated proxy for postsynaptic strengthening of excitatory transmission (Meye et al., 2015). The AMPAR/NMDAR ratio significantly, but transiently, augmented in learner mice compared to control mice (Figure 2A). Namely, it was larger 24 hours after training session two (III), and positively correlated with avoidance performance (Figure 2A and Figure 2B). However, AMPAR/NMDAR ratios were lower and comparable between experimental groups 24 hours after session three and four, as well as after session one, indicating the transient nature of this plasticity (Figure 2A).

The increased AMPAR/NMDAR ratio detected 24 hours after session two can occur via enhanced AMPAR function/number or alternatively via reduction of NMDAR function/number (Mameli et al., 2011). To probe the contribution of each glutamate receptor type during avoidance learning we used uncaging of MNI-glutamate onto LHb dendrites. At +40 mV, a brief (1.5 msec) flash of 405 nm UV-light evoked a composite response (AMPAR– and NMDAR–mediated). Isolation of AMPARs and NMDARs currents unraveled higher AMPAR/NMDAR ratios in learner mice, similarly to the results obtained with extracellular stimulation (Figure 2C). Comparison of AMPAR and NMDAR absolute currents revealed a significant upward shift of AMPAR-EPSCs amplitudes, while NMDAR responses remained comparable across experimental groups (Figure S2A). Avoidance learning (at session III), however, did not alter EPSCs evoked by high frequency trains of synaptic stimulation, indicating unaltered presynaptic glutamate release (Figure S2B). Altogether, these data suggest that cue-punishment association, and the consequent development of avoidance, occurs along with a postsynaptic potentiation of AMPAR-dependent transmission onto LHb neurons. We reasoned that if learning requires such an LTP-like process, animals undergoing avoidance learning would show occluded LTP *in vitro*. Pairing high frequency extracellular stimulation with postsynaptic depolarization (1 sec at 20 mV) led to LTP in slices from control (and naïve) mice (Figure 2D and Figure S2C). This phenomenon required NMDARs, as it was abolished by the presence of the NMDAR antagonist AP5 (Figure S2C). The pairing protocol failed, however, to induce LTP in slices obtained from mice

undergoing avoidance learning (III; Figure 2D). Altogether, cue-punishment association and avoidance occur along with transient LTP of postsynaptic AMPAR transmission.

Pathway specificity of avoidance learning-driven plasticity

The lateral hypothalamus (LH), the medial VTA (mVTA) and the entopeduncular nucleus (EPN) i. project glutamate-releasing axons to the LHb, ii. activate AMPARs and NMDARs, and iii. promote LHb neuronal firing to drive aversive behaviors (Root et al., 2014; Shabel et al., 2012; Stamatakis and Stuber, 2016). Importantly, unexpected punishments engage the LH-to-LHb pathway to trigger LHb neuronal excitation (Lecca et al., 2017). We examined the possibility that synaptic potentiation in the LHb during avoidance also presents circuit specificity. To this end, we virally expressed the excitatory opsin CoChR (CoChR–eGFP; Klapoetke et al., 2014) into the LH, mVTA, or the EPN (Figure 3A). Whole-cell recordings within the fluorescent terminal fields in the LHb, from all these inputs, confirmed the excitatory nature of opto–currents (Figure 3B and Figure S2D). Twenty-four hours after training session one and two (II and III), AMPAR/NMDAR ratios at LH-LHb synapses were significantly larger in learner compared to control mice, matching the initial progression of avoidance learning. Instead, optically-driven mVTA- and EPN-LHb AMPAR/NMDAR ratios were comparable between groups (Figure 3B and Figure S2E). Notably, AMPAR/NMDAR in control condition were highly variable across inputs indicating pathway-specific postsynaptic properties. In addition, a fear conditioning protocol, where CS-US association occurs but in an inescapable condition, failed to change LH-LHb AMPAR/NMDAR ratios (Figure S2F).

We find that an optical-HFS protocol at LH inputs paired with postsynaptic depolarization employing the fast opsins CoChR and Chrimson (Klapoetke et al., 2014) led to LTP in control mice (Figure S2G). This phenomenon was absent at EPN inputs and occluded in learner mice (Figure S2G and Figure S2H). These data support the notion that, i. at LH-LHb synapses, AMPA/NMDA ratio increases along with LTP (Figure S2I) and ii. learning-driven AMPAR potentiation is circuit specific.

To corroborate these results and visualize the locus of expression for avoidance-driven AMPAR potentiation, we employed freeze-fracture replica immunolabeling (Schönherr et al., 2016). Combined with infusion of rAAV2-hSyn-CoChR-eGFP, this approach allows the quantification of membrane AMPARs specifically at synapses formed by LH axons to LHb post-synaptic neurons (Figure 3C). AMPARs (GluA1–4) gold immunolabeling showed no overall difference in density between learner and control mice. However, in learner mice (24 hours after session 2) a larger fraction of particles (receptors) within the broader PSD areas was observed compared to control animals (Figure 3C). Altogether, this suggests that a larger postsynaptic membrane pool of AMPARs underlies the potentiation of LH-to-LHb excitatory synapses during avoidance learning.

Required circuit and mechanism for avoidance learning.

We next aimed to probe the necessity of LH inputs for avoidance learning. We tested LH to LHb projections requirement by optically reducing their function. We transduced LH neurons with a light-driven chloride pump (orange-red spectrum of activation) via infusion of rAAV2-JAWS-eGFP (Figure 4A). Four weeks later, we prepared acute brain slices and found that 584 nm light reduced EPSCs within the LHb (Figure S3A). Next, we recorded foot-shock-driven LH-dependent LHb excitation using single units in anesthetized mice (Lecca et al., 2017). Light at 638 nm reduced foot-shock excitation in JAWS-expressing mice, but not in GFP-control animals (Figure S3B). These experiments also revealed that light off failed to induce any rebound excitation (Figure S3B). Thus, JAWS activation efficiently reduces presynaptic function of LH terminals onto the LHb. Next, we chronically implanted JAWS–expressing mice with a single fiber optic directed just above the LHb (Figure S3C). We reasoned that breaking the contingency between CS and US by functionally limiting LH-LHb projections would impair the formation of punishment-predictive cues. Shining light at 638 nm to silence LH-to-LHb terminals during CS presentation reduced avoidance learning (Figure 4B). This highlights the necessary role of the LH-LHb projection for the acquisition of avoidance behavioral strategy.

While this provides insights for the circuit requirement of avoidance, it leaves open the existence of causality between AMPAR strengthening and behavior. We predicted that synaptic potentiation of AMPARs is an essential mechanism for avoidance learning. To test this, we employed Chromophore-Assisted Light Inactivation with eosin (CALI) to inactivate GluA1-containing AMPARs with precise temporal and spatial resolution (Takemoto et al., 2017). Monoclonal antibodies against an extracellular domain of GluA1 (236–286 aa) chemically labeled with eosin produce oxygen singlets in response to 532 nm laser light, thereby damaging synaptic GluA1–AMPARs (CALI-GluA1) (Takemoto et al., 2017). Notably, CALI-GluA1 efficiently targets and impairs newly inserted AMPARs, which represent a receptor pool more labile and less anchored to the scaffolding complex (Malinow and Malenka, 2002; Takemoto et al., 2017). To examine the efficiency of CALI-GluA1 in the LHb, we locally infused the antibody in control and learner mice 4-5 hours prior session two (Figure 4C). One hour after session two, we found that continuous 532 nm laser light onto slices reduced AMPAR currents solely in learner mice (Figure 4C). This suggests that CALI-GluA1 rapidly and efficiently diminishes AMPAR transmission in animals undergoing avoidance learning. Therefore this intervention offers an opportunity to test causality between strengthened AMPAR transmission and avoidance learning with fine temporal and spatial precision.

In order to achieve this, we initially trained a set of mice during session one. The following day, the same mice underwent infusion of either CALI-GluA1 or a control antibody (anti-Myc-eosin, Ctrl-Ab) into the LHb (Takemoto et al., 2017). Mice were then implanted with a fiber optic, and experienced training session two (Figure S3D). One hour post training we exposed the injected area to 532 nm continuous illumination. The following day, mice were tested on session day three (Figure 4D). All injected animals (“Learners“) progressively increased avoidance performance during the initial two sessions (Figure 4D). Illumination left the progression of learning intact in mice infused with Ctrl-Ab. In contrast, CALI-GluA1-L mice failed to further improve their avoidance performance, and exhibited a significant reduction in cue-driven

avoidance compared to Ctrl-Ab-L mice. CALI-GluA1 did not affect the behavior of control mice (Figure 4D). When examining AMPAR/NMDAR ratio in LHb-containing slices from these same animals, we found that Ctrl-Ab-L mice exhibited high AMPAR/NMDAR ratios. In contrast, CALI-GluA1-L mice presented a significantly lower AMPAR/NMDAR, comparable to those from CALI-GluA1 control mice. Altogether, this indicates that GluA1-mediated synaptic potentiation in the LHb is a requirement for proper avoidance.

Discussion

LHb neurons respond to unpredicted punishments. Here we show that also punishment-predictive cues excite LHb neuronal population during avoidance learning. This phenomenon parallels the expression of an LTP-like process at lateral hypothalamic-to-LHb excitatory synapses, a synaptic substrate necessary for avoidance.

Synaptic basis of avoidance

We describe that during avoidance learning a transient enhancement of excitatory synaptic transmission onto LHb neurons occurs, as a result of AMPAR enrichment at LH-to-LHb synapses. In addition, LHb neurons of learner mice did not show, in contrast to control animals, HFS-LTP in acute brain slices. This suggests that during the steep initial phase of avoidance learning, LH-to-LHb excitatory synapses undergo potentiation. Such synaptic potentiation, however, does not occur during CS-US association in an inescapable context, an encoding primarily mediated by amygdala neuronal populations (Ciocchi et al., 2010).

Short-term and long-term changes in excitatory transmission within the LHb are also instrumental for punishment-mediated innate escape as well as for behavioral despair in depressive states (Lecca et al., 2017; Li et al., 2013). Altogether, these data highlight the contribution of glutamatergic transmission for precise LHb-dependent neuronal encoding, ultimately leading to avoidance learning.

A feature of this study is the input-specific expression of avoidance learning-induced plasticity. Afferents from the LH, the mVTA and the EPN onto the

LHb contribute to aversion processing, and are sufficient to drive aversive behaviors (Root et al., 2014; Shabel et al., 2012; Stamatakis and Stuber, 2016). The avoidance learning-mediated adaptations including the increase in AMPAR/NMDAR ratio, occlusion of LTP, and higher AMPARs membrane expression, specifically occur at LH-to-LHb synapses. In addition, silencing LH-to-LHb terminals diminishes avoidance behaviors. What renders the LH-to-LHb an essential substrate for avoidance? CREB phosphorylation, crucial for learning processes, occurs during avoidance in the hypothalamus (Saha and Datta, 2005; Won and Silva, 2008). Furthermore, impairment of the orexin signaling in the hypothalamus disrupts taste aversion learning (Mediavilla et al., 2011). Lastly, LH neurons mediate unpredicted foot-shock-driven LHb neuronal excitation, and their terminal activation in LHb guide real-time place aversion (Lecca et al., 2017). Altogether, LH-driven excitatory transmission onto LHb neurons represents a fundamental substrate contributing to the encoding of both unpredicted aversion and prediction of punishment. Glutamate release onto LHb neurons remains unaffected during progression of learning, suggesting the absence of plastic mechanisms in upstream structures. However, the induction mechanisms (i.e. coincident detection and/ or precise firing patterns) endowing LH terminals to establish synaptic potentiation onto LHb synapses remain yet to be clarified. Recent data point to the medial septum as a source of sensory information to the LHb (Zhang et al., 2018). Neuromodulators are released during salient experiences in several brains structures, including the LHb (Lecca et al., 2014). These may represent two potential gating candidates to mechanistically trigger the LTP-like processes that guide avoidance learning. Our data do not rule out a potential contribution of *i*. alternative inputs impinging onto the LHb and *ii*. other type of neurotransmission during discrete phases of avoidance.

The local and temporally-restricted inactivation of GluA1-AMPARs resets synaptic strengthening thereby impairing avoidance behavior. This supports a causal role of AMPAR-mediated potentiation for establishing cue-punishment association and subsequent avoidance learning. Notably, we report that CALI-GluA1 mediates reduction of EPSCs solely in the learner group. This is consistent with previous results suggesting that AMPARs participating to

synaptic potentiation during learning are more susceptible to inactivation (Takemoto et al., 2017). This may result from LTP-driven insertion of a labile AMPAR pools or unsilencing of silent synapses (Groc et al., 2006; Malinow, 2003). Altogether, these results favor the notion that punishment predictive memories can form through AMPAR-mediated LTP-like processes.

Evolution of plasticity during prediction learning

A signature of the reported synaptic potentiation during avoidance is its transient nature, as it occurs during a restricted time window, namely during the steepest portion of cue-punishment learning. During this phase mice exhibited the largest change in number of avoidances compared to the previous session. Therefore, such synaptic plasticity may facilitate cue-punishment association and the consequent acquisition of avoidance. However, the extent of synaptic potentiation, reflected by the AMPAR/NMDAR ratio, returned back to baseline levels at later sessions. This inverted U-shape of learning-driven potentiation suggests that this process may not contribute to the maintenance of the learned avoidance behavior. It is therefore plausible that persistent cue-punishment memories are mediated by different mechanisms within the LHb or stored elsewhere than the LHb (i.e. monoaminergic nuclei) (Wenzel et al., 2018). Notably, such phenomenon presents striking similarities with cue-reward learning in dopamine neurons of the VTA (Stuber et al., 2008). In the midbrain, transient synaptic strengthening of AMPAR neurotransmission has been proposed as a leading substrate to enable reward prediction.

Altogether, these data support that in the LHb, and more broadly within neuronal circuits of motivation, the transient enhancement in synaptic strength during the acquisition of avoidance (or reward) learning may transform neutral stimuli into punishment– (or reward–) predictive stimuli. This provides insights on how the brain resolves novel cue-stimulus associations.

Acknowledgements

We thank M. Carta, D. Dupret, L. Neukomm, F.J. Meye and the members of the Mameli laboratory for comments on the manuscript. We thank the Bellone

and Tan laboratories for viral constructs and technical assistance. This work was supported by the Austrian Science Fund Sonderforschungsbereich grant F44-17 to F.F., ERC StG SalienSy 335333, the Swiss National Funds 31003A and Vaud Canton to M.M.

Author contributions

M.T and M.M. conceptualized the project, performed and analyzed the electrophysiological recordings and behavior. M.T. and S.L. performed and analyzed in vivo photometry data. A.N.P. performed electrophysiological recordings. A.L.L. and M.C. performed in vivo electrophysiology experiments. H.H. and F.F. performed and analyzed the electron microscopy data. K.T. and T.T. provided tools for CALI. M.M. and M.T. wrote the manuscript with the help of all authors.

Declaration of interests

The authors declare no competing interests.

References

Ciocchi S., Herry C., Grenier F., Wolff S.B., Letzkus J.J., Vlachos I., Ehrlich I., Sprengel R., Deisseroth K., Stadler M.B., Müller C., Lüthi A. (2010) Encoding of conditioned fear in central amygdala inhibitory circuits. Nature *11*, 277-82.

Groc, L., Gustafsson, B., and Hanse, E. (2006). AMPA signalling in nascent glutamatergic synapses: there and not there. Trends Neurosci *29*, 132-139.

Klapoetke, N. C., Murata, Y., Kim, S. S., Pulver, S. R., Birdsey-Benson, A., Cho, Y. K., Morimoto, T. K., Chuong, A. S., Carpenter, E. J., Tian, Z., Wang, J., Xie, Y., Yan, Z., Zhang, Y., Chow, B. Y., Surek, B., Melkonian, M., Jayaraman, V., Constantine-Paton, M., Wong, G. K., and Boyden, E. S. (2014). Independent optical excitation of distinct neural populations. Nat Methods *11*, 338-346.

Lecca, S., Meye F.J., Mameli M. (2014). The lateral habenula in addiction and depression: an anatomical, synaptic and behavioral overview. Eur J Neurosci *39*, 1170-8.

Lecca, S., Meye, F. J., Trusel, M., Tchenio, A., Harris, J., Schwarz, M. K., Burdakov, D., Georges, F., and Mameli, M. (2017). Aversive stimuli drive hypothalamus-to-habenula excitation to promote escape behavior. Elife *6*,

Lecca, S., Pelosi, A., Tchenio, A., Moutkine, I., Lujan, R., Hervé, D., and Mameli, M. (2016). Rescue of GABAB and GIRK function in the lateral habenula by protein phosphatase 2A inhibition ameliorates depression-like phenotypes in mice. Nat Med *22*, 254-261.

LeDoux, J. E., Moscarello, J., Sears, R., and Campese, V. (2017). The birth, death and resurrection of avoidance: a reconceptualization of a troubled paradigm. Mol Psychiatry *22*, 24-36.

Li, B., Piriz, J., Mirrione, M., Chung, C., Proulx, C. D., Schulz, D., Henn, F., and Malinow, R. (2011). Synaptic potentiation onto habenula neurons in the learned helplessness model of depression. Nature *470*, 535-539.

Malinow, R. (2003). AMPA receptor trafficking and long-term potentiation. Philos Trans R Soc Lond B Biol Sci *358*, 707-714.

Malinow, R., and Malenka, R. C. (2002). AMPA receptor trafficking and synaptic plasticity. Annu Rev Neurosci *25*, 103-126.

Mameli, M., Bellone, C., Brown, M. T., and Lüscher, C. (2011). Cocaine inverts rules for synaptic plasticity of glutamate transmission in the ventral tegmental area. Nat Neurosci *14*, 414-416.

Matsumoto, M., and Hikosaka, O. (2007). Lateral habenula as a source of negative reward signals in dopamine neurons. Nature *447*, 1111-1115.

Mediavilla, C., Cabello, V., and Risco, S. (2011). SB-334867-A, a selective orexin-1 receptor antagonist, enhances taste aversion learning and blocks taste preference learning in rats. Pharmacol Biochem Behav *98*, 385-391.

Meye, F. J., Valentinova, K., Lecca, S., Marion-Poll, L., Maroteaux, M. J., Musardo, S., Moutkine, I., Gardoni, F., Huganir, R. L., Georges, F., and Mameli, M. (2015). Cocaine-evoked negative symptoms require AMPA receptor trafficking in the lateral habenula. Nat Neurosci *18*, 376-378.

Nabavi, S., Fox, R., Proulx, C. D., Lin, J. Y., Tsien, R. Y., and Malinow, R. (2014). Engineering a memory with LTD and LTP. Nature *511*, 348-352.

Root, D. H., Mejias-Aponte, C. A., Qi, J., and Morales, M. (2014). Role of glutamatergic projections from ventral tegmental area to lateral habenula in aversive conditioning. J Neurosci *34*, 13906-13910.

Saha, S., and Datta, S. (2005). Two-way active avoidance training-specific increases in phosphorylated cAMP response element-binding protein in the dorsal hippocampus, amygdala, and hypothalamus. Eur J Neurosci *21*, 3403-3414.

Schönherr, S., Seewald, A., Kasugai, Y., Bosch, D., Ehrlich, I., and Ferraguti, F. (2016). Combined Optogenetic and Freeze-fracture Replica Immunolabeling to Examine Input-specific Arrangement of Glutamate Receptors in the Mouse Amygdala. J Vis Exp

Shabel, S. J., Proulx, C. D., Trias, A., Murphy, R. T., and Malinow, R. (2012). Input to the lateral habenula from the basal ganglia is excitatory, aversive, and suppressed by serotonin. Neuron *74*, 475-481.

Stamatakis, A. M., and Stuber, G. D. (2012). Activation of lateral habenula inputs to the ventral midbrain promotes behavioral avoidance. Nat Neurosci *15*, 1105-1107.

Stamatakis, A. M., Van Swieten, M., Basiri, M. L., Blair, G. A., Kantak, P., and Stuber, G. D. (2016). Lateral Hypothalamic Area Glutamatergic Neurons and Their Projections to the Lateral Habenula Regulate Feeding and Reward. J Neurosci *36*, 302-311.

Stuber, G. D., Klanker, M., de Ridder, B., Bowers, M. S., Joosten, R. N., Feenstra, M. G., and Bonci, A. (2008). Reward-predictive cues enhance excitatory synaptic strength onto midbrain dopamine neurons. Science *321*, 1690-1692.

Takemoto, K., Iwanari, H., Tada, H., Suyama, K., Sano, A., Nagai, T., Hamakubo, T., and Takahashi, T. (2017). Optical inactivation of synaptic AMPA receptors erases fear memory. Nat Biotechnol *35*, 38-47.

Valentinova, K., and Mameli, M. (2016). mGluR-LTD at Excitatory and Inhibitory Synapses in the Lateral Habenula Tunes Neuronal Output. Cell Rep *16*, 2298-2307.

Wang, D., Li, Y., Feng, Q., Guo, Q., Zhou, J., and Luo, M. (2017). Learning shapes the aversion and reward responses of lateral habenula neurons. Elife *6*.

Wenzel, J. M., Oleson, E. B., Gove, W. N., Cole, A. B., Gyawali, U., Dantrassy, H. M., Bluett, R. J., Dryanovski, D. I., Stuber, G. D., Deisseroth, K., Mathur, B. N., Patel, S., Lupica, C. R., and Cheer, J. F. (2018). Phasic

Dopamine Signals in the Nucleus Accumbens that Cause Active Avoidance Require Endocannabinoid Mobilization in the Midbrain. Curr Biol *28*, 1392-1404.e5.

Won, J., and Silva, A. J. (2008). Molecular and cellular mechanisms of memory allocation in neuronetworks. Neurobiol Learn Mem *89*, 285-292.

Zhang G.W., Shen L., Zhong W., Xiong Y., Zhang L.I., Tao H.W. (2018). Transforming Sensory Cues into Aversive Emotion via Septal-Habenular Pathway. Neuron *99*, 1016-1028.

Figure legends

Figure 1 Excitation of LHb neurons by aversion-predictive cues develops during avoidance learning

(A) Behavioral protocol; time-course and bar graph with scatterplot illustrating avoidance rate along 5 sessions (controls (C, black) $n_{animals}$=7, learners (L, red) $n_{animals}$=9; Two-way repeated measures ANOVA, main effect of training protocol, session, and interaction, ***P<0.001; % US received: session 1, C=100%, L=83.4±3.8%; session 5, C=100±0 %, L=13.3±3.2%, L: session 1 vs session 5, t-test, $t_{8=}$18.4 ***p<0.001).

(B) Protocol, injection site, and image illustrating GCamP6f expression in the LHb (500 µm); Sample heat map and traces (100 photons, 10 s) of normalized fluorescence signal after CS (0-10 s, blue) and US (onset 10s) across the 30 trials on day 1, 3 and 5.

(C) Box and scatter plot summarizing the normalized fluorescence (Max Photons/Baseline) upon CS across sessions (n=9, RM One-way ANOVA, Dunnett's D1 vs D5 $q_{8=}$3.3 *p=0.03).

(D) Scatter plot and correlation analysis for avoidance scores and the CS/US fluorescence across the sessions (n=9, Spearman r=0.448, *p=0.047, R^2 represents the goodness of fit).
Data are represented with box plots (median and quartiles) or mean±SEM.
See also Figure S1.

Figure 2 Transient synaptic potentiation onto LHb neurons during avoidance.

(A) Timeline and sample traces (10 pA, 20 ms) representing AMPAR and NMDAR-EPSCs (+40 mV). Box and scatter plot of the AMPAR/NMDAR ratios (session I, 1h after session 1: controls (C, black) 1.7±0.4, $n_{cells}/_{animals}$=7/3; learners (L, red) 1.6±0.4, $n_{cells}/_{animals}$=7/3; t-test, $t_{12=}$0.29 p>0.05. II, 24h after session 1: C 1.5±0.3, $n_{cells}/_{animals}$=9/3; L 1.8±0.3, $n_{cells}/_{animals}$=18/4; t-test, $t_{25=}$0.87 p>0.05. III, 24h after session 2: C 1.1±0.2, $n_{cells}/_{animals}$=10/6; L

3.0±0.6, $n_{cells}/_{animals}$=16/7; t-test, t_{24}=2.5 *p=0.02. IV, 24h after session 3: C 1.5±0.3, $n_{cells}/_{animals}$=8/2; L 2.4±0.4, $n_{cells}/_{animals}$=13/2; t-test, t_{19}=1.58 p>0.05. V, 24h after session 4: C 1.5±0.2, $n_{cells}/_{animals}$=8/4; L 1.4±0.3, $n_{cells}/_{animals}$=9/4; t-test, t_{15}=0.26 p>0.05).

(B) Avoidance scores plotted in function of AMPAR/NMDAR ratios (Learners, empty circles, single cells; filled circles, average value/mouse; session I, II, III) (correlation value/mouse; Spearman r=0.766 **p=0.003, R^2 represents the goodness of fit).

(C) Same as A, but with MNI-Glutamate uncaging (controls (C, black) 0.6±0.2, $n_{cells}/_{animals}$=8/2; learners (L, red) 1.7±0.4, $n_{cells}/_{animals}$=11/3; Mann-Whitney, U=19 *p=0.04).

(D) Amplitude versus time plot, and sample traces (50 pA, 10 ms) of EPSCs before (light line) and after (dark line) HFS-pairing protocol (average $EPSC_{34\text{-}36\ min}$: controls (C, black), 208.1±38.4 $n_{cells}/_{animals}$=7/3; learners (L, red), 107.5±11.8, $n_{cells}/_{animals}$=7/3; t-test, t_{12}=2.5 **p=0.03).
Data are represented with box plots (median and quartiles) or mean±SEM.
See also Figure S2.

Figure 3 Learning-driven potentiation at hypothalamic-to-habenula projections.
(A) Timeline and representative images for CoChR expression in LH, mVTA, EPN and LHb terminals (500 µm).

(B) Sample traces at session III (LH 50 pA, 20 ms, mVTA, 10 pA, 20 ms; EPN 50 pA, 20 ms), Box- and scatter-plot of the optical AMPA/NMDA ratios (LH, session II: C 0.8±0.2, $n_{cells}/_{animals}$=9/2; L 1.8±0.3, $n_{cells}/_{animals}$=12/2; t_{19}=2.4 p=0.03; session III: C 1.3±0.2, $n_{cells}/_{animals}$=10/5; L 2.2±0.3, $n_{cells}/_{animals}$=18/6; t-test, t_{26}=2.2 p=0.04; session IV: C 1.0±0.2, $n_{cells}/_{animals}$=10/2; L 1.5±0.2, $n_{cells}/_{animals}$=14/2; t-test, t_{22}=1.4 p>0.05; session V: C 1.1±0.2, $n_{cells}/_{animals}$=9/2; L 0.8±0.1, $n_{cells}/_{animals}$=10/2; t-test, t_{17}=1.0 p>0.05. mVTA, session III: controls (C, black) 1.5±0.2, $n_{cells}/_{animals}$=8/5; learners (L, red) 1.6±0.5, $n_{cells}/_{animals}$=8/4; t-

test, $t_{14=}$0.13 p>0.05. EPN, session III: C 2.7±0.7, $n_{cells}/_{animals}$=6/3; L 2.9±0.6, $n_{cells}/_{animals}$=8/3; t-test, $t_{12=}$0.3 p>0.05.).

(C) Timeline and representative images of Freeze-Fracture Replica Immunolabeling for AMPARs at LH-to-LHb synaptic contacts (200 nm). Portion of a LH axon terminal (protoplasmic face in light green, 10 nm gold particle of CoChR-GFP, white arrowheads) apposed to a LHb dendritic shaft. AMPARs (5 nm gold particles, black arrows) were observed in the postsynaptic membrane specialization (PSD). Box and scatter plot of averaged density (5 nm gold particles/µm^2) (controls (C, black), 1220.6±79, $n_{counts/animals}$=179/6; learners (L, red), 1272.3±33.5, $n_{counts/animals}$=192/6; Mann-Whitney, U=18 p>0.05).
Data are represented with box plots (median and quartiles).
Third-order polynomial fitting of AMPARs number versus normalized PSD area (Control vs Learners, $n_{animals}$=6/group; $F_{4,361=}$15 p<0.001, R^2 indicates goodness of fit). See also Figure S2.

Figure 4 Avoidance learning requires LH-to-LHb projections and AMPARs potentiation.
(A) Fiber implant and infusion of rAAV-CAG-JAWS-eGFP; representative images for JAWS expression (500 µm).

(B) Training protocol and behavioral performance during training (Learners-control virus (L-Ctrl, red, n=8), Learners-JAWS (L-JAWS, green, n=5); Two-way repeated measures ANOVA, main effect of virus, session, and interaction ($F_{2, 22}$=3.8, p=0.04).

(C) Schematic of CALI approach. Amplitude versus time plot of EPSCs (50 pA, 10 ms) before (light) and after (dark) light exposure (532 nm) (average $EPSC1_{8\text{-}22\ min}$: CALI-GluA1-C (black) 98.2±3.7 $n_{cells/animals}$=6/4; CALI-GluA1-L (red) 79.7±1.9, $n_{cells/animals}$=6/4; t-test, $t_{10=}$4.4 **p=0.01).

(D) Timeline of avoidance performance (Infusion 4h prior session 2, light 1h post session 2). Average shuttles during CS at session 3: control mice CALI-

GluA1 (CALI-GluA1-C, black) 3.2±0.7; learner mice control antibody (Ctrl-Ab-L, red) 18.3±1.6; learner mice CALI-GluA1 (CALI-GluA1-L, green) 12.8±0.7; One-Way ANOVA $F_{(2,16)=}47$, **p<0.01.

(E) Sample traces (20 pA, 20 ms) representing AMPAR and NMDAR-EPSCs 12h after behavioral testing. Box- and scatter-plot of the AMPAR/NMDAR ratios (CALI-GluA1-C 1.3±0.8, $n_{cells/animals}$=8/3; Ctrl-Ab-L 2.6±0.3, $n_{cells/animals}$=8/2; CALI-GluA1-L 1.1±0.1, $n_{cells/animals}$=8/3; One-Way ANOVA $F_{(2,21)}$= 13.78, **p<0.01).
Data are represented with box plots (median and quartiles) or mean±SEM.
See also Figure S3.

STAR Methods

Contact for Reagent and Resource Sharing

Further information and requests for resources and reagents should be directed to and will be fulfilled by the Lead Contact, Manuel Mameli (manuel.mameli@unil.ch).

Experimental Model and Subject Details

Male naive mice (C57Bl6/J; 4–12 weeks) were group-housed (three to five per cage) on a 12:12 h light cycle (lights on at 7 a.m.) with food and water ad libitum. All procedures aimed to fulfill the 3R criterion and were approved by the Veterinary Offices of Vaud (Switzerland; License VD3171).

Method details

Stereotactic injections

Mice were anesthetized with ketamine (150 mg kg^{-1}) and xylazine (100 mg kg^{-1}) (Veterinary office University of Lausanne) and were placed on a stereotactic frame (Kopf, Germany). Bilateral injections obtained through a glass needle of 200-400 nl volume were performed at a rate of approximately 100 nl min^{-1}. The injection pipette was withdrawn from the brain 10 min after the infusion. Injections were performed using the following coordinates: lateral hypothalamus (LH: −1.25 mm posterior to bregma, 0.95 mm lateral, −5.1 mm ventral from pia); entopeduncular nucleus (EPN: −1.25 mm posterior to bregma, 1.80 mm lateral, −4.65 mm ventral); medial VTA (mVTA: −2.2 mm posterior to bregma, 0.3 mm lateral, −4.8 mm ventral); lateral habenula (LHb: −1.35 mm posterior to bregma, 0.45 mm lateral, −3.1 mm ventral). Animals were allowed to recover for a minimum of 3 weeks before the recordings.

Viral constructs employed in the study: rAAV2.5–*h*Syn–CoChR–eGFP (University of North Carolina viral vector core, USA; titer: 1×10^{12} gc/ml); AAV5-*h*Syn-Chrimson-tdTomato (University of Pennsylvania viral vector core; titer: 7×10^{12} gc/ml). rAAV2.2–CAG–JAWS–GFP (Vector biolabs, USA; titer: 7×10^{12} gc/ml); rAAV2.5–*h*Syn–GCaMP6f, rAAV2.1–CAG–tdTomato (University

of Pennsylvania viral vector core; titer: 5×10^{12} gc/ml and 1.19×10^{13} gc/ml). The injection sites were examined for all experiments and only data from animals with correct injections were included.

Slice electrophysiology

The mice were anesthetized (ketamine/xylazine; 150 mg/100 mg kg^{-1}), sacrificed, and their brains were transferred in ice-cold carbogenated (95% O_2/5% CO_2) solution, containing (in mM) choline chloride 110; glucose 25; $NaHCO_3$ 25; $MgCl_2$7; ascorbic acid 11.6; sodium pyruvate 3.1; KCl 2.5; NaH_2PO_4 1.25; $CaCl_2$0.5. Coronal brain slices (250 µm thickness) were prepared and transferred for 10 min to warmed solution (34 °C) of identical composition, before they were stored at room temperature in carbogenated artificial cerebrospinal fluid (ACSF) containing (in mM) NaCl 124; $NaHCO_3$ 26.2; glucose 11; KCl 2.5; $CaCl_2$ 2.5; $MgCl_2$ 1.3; NaH_2PO_4 1. During recordings, slices were immersed in ACSF and continuously superfused at a flow rate of 2.5 ml min^{-1} at 30 °C. Neurons were patch-clamped using borosilicate glass pipettes (2.7–4 MΩ; Phymep, France) under an Olympus-BX51 microscope (Olympus, France). For voltage or current clamp recordings, signal was amplified, filtered at 5 kHz and digitized at 10 kHz (Multiclamp 200B; Molecular Devices, USA). Data were acquired using Igor Pro with NIDAQ tools (Wavemetrics, USA). Access resistance was continuously monitored with a −4 mV step delivered at 0.1 Hz. Experiments were discarded if the access resistance increased by more than 20% during the recording.

Extracellular stimulation from AMPI ISO-Flex stimulator was delivered through glass electrodes placed in the LHb.

Light stimulation (470 nm 1 ms for CoChR experiments, 584 nm continuous for JAWS experiments) was delivered with a LED (CoolLed, UK) illumination system. We systematically tested for direct optically-driven currents (100 msec light) sporadically observed in regions receiving afferent inputs from the site of injection. In case a direct photo-current was found the cell was discarded.

A 532 nm laser (Integrated Optics, Lithuania) was used in the experiments for the in-vitro validation and in-vivo activation (2 min light exposure) of the CALI

strategy. For glutamate uncaging (4-methoxy-7-nitroindolinyl-caged L-glutamate 200µM, Tocris), a single-path photolysis head was connected to a solid-state laser (Rapp Optolectronics, Germany; 405 nm, duration 0.5 ms, diameter 3–5µm).

All recordings were made in voltage-clamp configuration, in picrotoxin-containing ACSF (100 µM). The stimulation intensity (electrical and light) was titered to obtain currents between ±50-300 pA. AMPA/NMDA ratios of evoked EPSC were obtained by AMPA-EPSC +40 mV/NMDA-EPSCs at +40 mV. I_{AMPAR} and I_{NMDAR} were pharmacologically isolated by the application of APV (100 µM), NBQX (20 µM), and by subsequent identification of the individual currents via digital subtraction. CALI and JAWS in-vitro validation experiments were performed in voltage clamp mode at -50 mV and light was applied continuously until the end of the experiment. The internal medium consisted of (in mM) cesium methanesulfonate 120, CsCl 10, HEPES 10, EGTA 10, creatine phosphate 5; Na2ATP 4; Na3GTP 0.4.

Long-term plasticity experiments were performed at -60 mV with an internal solution contained the following (in mM): K-gluconate 140; KCl 5; HEPES 10; EGTA 0.2; MgCl2 2; Na2ATP 4; Na3GTP 0.3; and creatine-phosphate 10. For the measurement of AMPA-EPSC$_{-60\ mV}$/NMDA-EPSCs$_{+40\ mV}$ before and after the LTP protocol, we used an internal solution containing the following (in mM): cesium methanesulfonate 130; 15 CsCl, 10 HEPES, 0.2 EGTA, 10 Creatine Phosphate, 4 ATP-Mg, 0.3 GTP-Na. The induction protocol for long-term plasticity consisted of 5 trains of 1s stimulation at 100 Hz, delivered at 0.1Hz, paired with somatic depolarization (+20 mV).

Data collection and analysis for the electrophysiology experiments were not performed blind to the conditions of the experiments.

In vivo electrophysiology

Recordings under anesthesia. For the JAWS validation in vivo, mice previously injected in the LH with rAAV2-CAG-JAWS-eGFP were anesthetized using isoflurane (Univentor, Malta. Induction: 2%; maintenance: 1-1.5%) and placed in the stereotaxic apparatus (Kopf, Germany). Their body temperature was maintained at 36 ± 1 °C using a feedback-controlled heating pad (CMA 450 Temperature controller, USA). An optrode was lowered at the

coordinates of LHb. Each cell was tested for its response to repetitive (every 5 s) shocks (0.5 s, 1.5 - 2 mA) delivered to the hind paw contralateral to the recording side. If excited the Fs response was re-tested while simultaneously shining the light (638nm, 10mW, 4 s). PSTHs and raster plots were built from 30 to 60 shocks and displayed using 10 ms bin width. A cell was considered excited when the mean number of action potentials/bin (bin length = 10 ms) in at least one of the four epochs (50 ms per epoch) after the shock inset was 2 times the Standard Deviation (SD) higher than baseline levels (the average number of action potentials/bin in the 2 s period before the shock). The duration of the response was calculated from the latency to the first of at least 5 consecutive bins not different than the baseline + 2SD. The magnitude of the response was obtained subtracting the baseline firing rate to the firing during the duration of the shock response.
At the end of each experiment, the electrode placement was determined with an iontophoretic deposit of pontamine sky blue dye (1 mA, continuous current for 5 min). Brains were then rapidly removed and fixed in 4% paraformaldehyde solution. The position of the electrodes was identified with a microscope on coronal section sections (100 µm). Only recordings in the correct area were considered for analysis.

For awake in vivo recordings, mice were implanted with a custom stainless steel headbar for head fixation. The scalp was removed and skull scraped clean and dry using a scalpel. LHb sites (AP, lateral, in mm, from bregma: −1.4, 0.45) were marked with sharpie pen on the skull and covered with a drop of silicone elastomer (Kwik-Cast; WPI). Cyanoacrylate glue (Vetbond, 3M) was lightly dabbed on the skull. Then, the headbar was levelled flat and lowered to touch lambda, covered with dental adhesive (C and B Metabond, Parkell) and secured with dental cement (Jetkit, Lang). Only a thin layer of cement was applied above the marked VM sites.
After at least 3 days of recovery, mice were habituated to head fixation in a 3-cm-wide acrylic cylinder for 10 min twice a day. In parallel, mice were trained for four days in the active avoidance paradigm. After the fourth training session, mice were anesthetized, dental cement and silicone above LHb were removed, and holes were drilled on the marked LHb locations. The

craniotomy was then covered in silicone elastomere. The next day, mice were headfixed for recordings, instead of the last behavior session.
After headfixation, the craniotomy was exposed and and electrode was lowered in the LHb (DV 2.3-3.2, from brain, in mm). Single unit activity was recorded extracellularly using glass micropipettes filled with 2% Chicago sky blue dissolved in 0.5 M sodium acetate (impedance 5-15 MΩ). Signal was filtered (band-pass 500–5000 Hz), pre-amplified (DAM80, WPI, Germany), amplified (Neurolog System, Digitimer, UK) and displayed on a digital storage oscilloscope (OX 530, Metrix, USA). Experiments were sampled on- and off-line by a computer connected to CED Power 1401 laboratory interface (Cambridge Electronic Design, Cambridge, UK) running the Spike2 software (Cambridge Electronic Design).
Single units were isolated and after recording baseline activity (3 minutes), each cell was tested for its response to CS presentation (25kHz, 80dB, 4s duration, random interval of 5-30s, 6 to 12 trials; recordings per single mouse lasted <90 min) delivered by a speaker placed nearby the mouse. PSTHs and raster plots were built using 100 ms bin normalized to a window of 2 sec baseline. For each cell we calculate the modulation index (CS firing – baseline firing / CS firing + baseline firing). A cell was considered excited or inhibited when the modulation index was larger than 0.1 or lower than -0.1, respectively.

Histology and immunofluorescence

Mice were anaesthetized and transcardially perfused with 4% paraformaldehyde (w/v) in 0.1 M phosphate buffered saline (PBS; pH 7.4). Coronal sections (100 µm) were cut with a vibratome. To examine fiber placement and for injection sites examination, we used an epifluorescent microscope (Zeiss) with a 5x and 10x objective. For immunofluorescence, the brain slices were incubated for 48h at 4°C in mouse anti-NeuN antibody (1:500, MAB377 Millipore) in PBS containing 0.3% Triton X and 5% normal goat serum. After extensive washes in PBS, the slices were incubated for 24h at 4°C with 647-Alexa-coupled secondary anti-mouse antibody (1:1000, Invitrogen). Images of the lateral habenula (3 fields/mouse) were acquired using a confocal microscope (TCS SP5 AOBS TANDEM, Leica) with a 20X

objective. The number of GCaMP6f and NeuN-positive neurons was counted. To identify the nature of cells expressing GCaMP6f, antigen retrieval was performed by incubating the brain slices in 50mM Na-citrate solution at 80°C for 30 minutes. Slices were rinsed, incubated 1h in a solution containing 0.3% Triton X and 5% normal goat serum, and then for 48h at 4°C in a cocktail of mouse anti-GAD67 antibody (1:250, MAB5406 Millipore) and goat anti-EAAC1 (1:250, MAB1520 Millipore) in PBS containing 5% normal goat serum. After extensive washes in PBS, the slices were incubated for 24h at 4°C with 555-Alexa-coupled secondary anti-goat antibody, and then 647-Alexa-coupled secondary anti-mouse antibody (1:1000, Invitrogen). Images of the LHb were acquired using a confocal microscope (TCS SP5 AOBS TANDEM, Leica) with a 20X and a 63X immersion objective. ImageJ software (version 1.6, http://rsb.info.nih.gov/ij/) was used for image processing.

Freeze fracture replica immunolabeling

Anesthetized mice were perfused transcardially using a peristaltic pump at a flow rate of 5 ml/min with 25 mM phosphate buffered saline solution (PBS) for 1 min, followed by ice cold 1% paraformaldehyde (PFA) and 15% saturated picric acid in 0.1 M phosphate buffer (PB) for 7 min. Coronal slices (130 mm thick) were cut using a vibrating microslicer (VT1000, Leica, Vienna, Austria) in 0.1 M PB. A region of the LHb was trimmed from the slices and immersed in graded glycerol (10-30% in 0.1 M PB) at 4°C overnight and frozen by a high pressure freezing machine (HPM 010; BAL-TEC, Balzers, Liechtenstein). Frozen samples were fractured using a double-replica table at -115°C and replicated by carbon deposition (5 nm thick), carbon-platinum (2 nm) and carbon (15 nm) with a freeze-fracture replica machine (BAF060; BAL-TEC). Tissue debris were dissolved with shaking at 80°C for 20 h in a solution containing 15 mM Tris-HCl (pH 8.3), 20% sucrose, and 2.5% SDS. The replicas were washed three times in 50 mM Tris-buffered saline (TBS, pH 7.4) containing 0.05% bovine serum albumin (BSA), 0.1% Tween-20, and 0.05% sodium azide and blocked with 5% BSA in washing buffer for 1 h at room temperature. Subsequently, they were incubated with primary antibodies for 3 overnights at 15°C. The primary antibodies were: guinea pig polyclonal IgG raised against the 717-754 amino acid residues common to all AMPA-R

subunits (diluted 1:200, Frontier Science Co. Ltd, Hokkaido, Japan, cat. no. panAMPAR-GP-Af580-1) and rabbit polyclonal IgG raised against the green fluorescent protein (GFP) from the jellyfish *Aequorea victoria* (diluted 1:1,000, Molecular Probes-Invitrogen, cat. no. A11122, Lot. no. 1356608). Antigen-antibody complexes were identified using secondary antibodies against the species of the first antibody and conjugated to gold particles of different size: goat anti-guinea pig IgG conjugated with 5 nm gold particles and goat anti-rabbit IgG conjugated with 10 nm gold particles (both diluted 1:30, British Biocell International, Cardiff, UK). Incubation was carried out overnight at 15°C. The labeled replicas were examined using a transmission electron microscope (CM-120; Philips).

Immunoparticles quantification

Images of excitatory postsynaptic specializations (PSD), identified by the presence of intramembrane particle (IMP) clusters on the exoplasmic face (E-face) accompanied by the protoplasmic face (P-face) of the presynaptic plasma membrane labeled by GFP immunoparticles, were captured at a magnification of 88,000 with a digital camera (Morada, Soft Imaging System; SIS). The PSD was demarcated freehand and the area was measured using the iTEM (SIS) or FIJI software (distributed under the General Public License). Immunoparticles within the PSD and those located outside but within 30 nm from the edge of the PSD were regarded as synaptic labeling, considering possible deviations of the immunoparticle from the antigen (Matsubara et al., 1996). The majority of analysis was performed on dendritic shafts as under our experimental conditions the vast majority of LHb spines were fractured at the neck and the PSD could not be exposed. Sampling and analysis of AMPAR density was performed by an investigator blind of the experimental groups. Data from both full and partial synapses were used since there was no significant difference ($p=0.31$, unpaired t-test) in AMPA-R density.

Fiber photometry

The fiber photometry measurements in this study were carried out by the ChiSquare $\square^2$-200 system (ChiSquare Biomaging, Brookline, MA). Briefly,

blue light from a 473-nm picosecond-pulsed laser (at 50 MHz; pulse width ~ 80 ps FWHM) was delivered to the sample through a single mode fiber. Fluorescence emission from the tissue was collected by a multimode fiber. The singlemode and multimode fibers were arranged side by side in a ferrule that is connected to a detachable multimode fiber implant. The emitted photons collected through the multimode fiber pass through a bandpass filter (FF01-550/88, Semrock) to a single-photon detector. Photons were recorded by the time-correlated single photon counting (TCSPC) module (SPC-130EM, Becker and Hickl, GmbH, Berlin, Germany) in the ChiSquare χ^2-200 system. Online analysis of photon counting was systematically employed to determine whether the fiber probe was correctly placed to detect fluorescent changes (photon count >300 photons). The experiments were replicated two to three times in the laboratory with different batches of mice.

Behavioral testing

Active avoidance. Behavioral tests were performed during the light phase. The active avoidance procedure (AA) was performed using a modified version of the Ugo Basile shuttle box apparatus. We substituted the door separating the two portions of the apparatus with two separate walls in order to allow the passage of optical fibers reaching the animal's head. The animals were handled daily by the experimenter for 3 days before the start of the behavioral tests. Mice were habituated to the testing room for a minimum of 30 minutes, and then a minimum of 10 minutes to the testing chamber. The training protocol consisted of a maximum of 5 sessions, 30 trials per session, 1 session/day. The protocol consisted in a random inter-trial interval (ITIs, min 20 s max 40 s) followed by a 10s ≈70dB 5Khz tone (conditioning stimulus, CS), immediately followed by a 0.3 mA footshock (unconditioned stimulus, US) delivered through the metallic floor grid. The foot shock had a maximal duration set to 25 s and was terminated when the animal shuttled to the opposite compartment, or prevented if the animal shuttled during the delivery of the CS. For electrophysiological experiments, the animals exposed to the training were excluded from further testing if they failed to avoid at least 5 trials during session 2. Control animals were subjected to a pattern of US designed to mimick the average experience of the learner group on each

specific session (1 to 5). The total duration of foot shock experienced in each session was scattered in episodes of 1, 2 or 3 s, and delivered not contingently to the US. For the control protocol, both CS and US were not-stoppable by shuttling to the opposite compartment.
For experiments employing JAWS in vivo, light was provided through a laser-coupled fiber optic at 638 nm. Light was applied during the entire presentation of the CS at a power of 15 mW at the tip of the fiber. For experiments using CALI (site of injection identified with flurobeads), a fiber optic delivered light (532 nm, 60 mW, 2 minutes) above the LHb.

Fear conditioning.
Animals underwent a fear conditioning procedure. Briefly, the animals were conditioned in the apparatus used for active avoidance. On the first day, they experienced 4 presentations of the CS (total CS duration of 30 s, 7.5 kHz, 80 dB; inter-trial interval: 20–180 s). On day 2 the CS was paired with a US (1-s foot shock, 0.6 mA, 5 CS+/US pairings; inter-trial interval: 20–180 s) at the offset of the CS. The animals were sacrificed for recordings 24h after the conditioning.

Drugs.
The drugs were obtained from Sigma (Switzerland), Tocris (Bristol, UK) and Hellobio (Bristol, UK). With the exception of picrotoxin and NBQX (DMSO, 0.01% final bath concentration), all drugs were dissolved in purified water.

Data analysis and statistics.
Online and offline analysis for electrophysiological data were performed using Igor Pro-6 (Wavemetrics, USA). Sample size was predetermined on the basis of published studies, experimental pilots and in-house expertise. Animals were randomly assigned to experimental groups. Compiled data are always reported and represented as box plots (median and quartiles) or mean±SEM, with single data points plotted (single cell for electrophysiology and single animal for behavioral experiments). Animals or data points were not excluded from analyses unless noted. Data distribution was tested for normality. When applicable, statistical tests were one-way ANOVAs, two-way ANOVAs, paired

or unpaired t-test. In case of not-normally distributed data, we used the Mann-Whitney and Friedman non-parametric test. Curve fitting was statistically tested with Pearson or Spearman tests. Testing was always performed two-tailed with $\alpha=0.05$.

KEY RESOURCES TABLE

TABLE FOR AUTHOR TO COMPLETE

Please upload the completed table as a separate document. ***Please do not add subheadings to the Key Resources Table.*** *If you wish to make an entry that does not fall into one of the subheadings below, please contact your handling editor. (**NOTE:** For authors publishing in Current Biology, please note that references within the KRT should be in numbered style, rather than Harvard.)*

KEY RESOURCES TABLE

REAGENT or RESOURCE	SOURCE	IDENTIFIER
Antibodies		
Anti-NeuN mouse	Millipore	Cat# MAB377; RRID: AB_2298772
647-Alexa anti-mouse	Invitrogen	Cat# A-21247; RRID: AB_141778
Anti-GAD67 mouse	Millipore	Cat# MAB5406; RRID: AB_2278725
Anti-EAAC1 goat	Millipore	Cat# MAB1520; RRID: AB_90732
panAMPA	Frontiers Science Company	Cat#: panAMPAR-GP-Af580-1
Anti-GFP Rabbit	Invitrogen	Cat#: A11122; RRID AB_221569
Goat anti-guinea pig IgG-5nm Gold particle	British Biocell International	Cat#: EM.GFAR5
Goat anti-rabbit IgG-10nm Gold particle	British Biocell International	Cat#: EM.GAR10
Bacterial and Virus Strains		
rAAV2.5–*h*Syn–CoChR–eGFP	UNC Vector Core	N/A
AAV5-*h*Syn-Chrimson-tdTomato	Addgene	Cat#: 59171
rAAV2.2–CAG–JAWS–GFP	Vector biolabs	N/A
rAAV2.5–*h*Syn–GCaMP6f	Addgene	Cat#: 100837
rAAV2.1–CAG–tdTomato	Addgene	Cat#: 59462
Chemicals, Peptides, and Recombinant Proteins		
Anti-GluA1-Eosin (Cali-GluA1)	Gift of T. Takahashi	
Anti-Myc-eosin (Control)	Gift of T. Takahashi	
D-AP5	Hello Bio	Cat#: HB0225
Picrotoxin	Hello Bio	Cat#: HB0506
NBQX disodium salt	Hello Bio	Cat#: HB0443

Figure 1

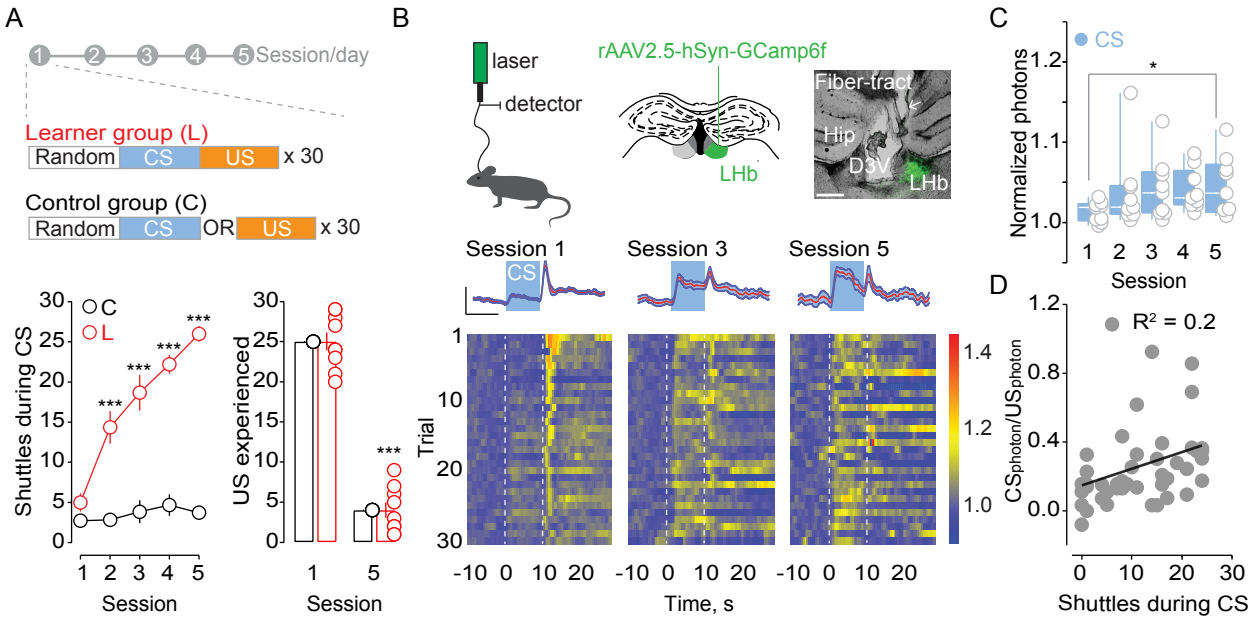

Trusel et al., Figure 1

Figure 2

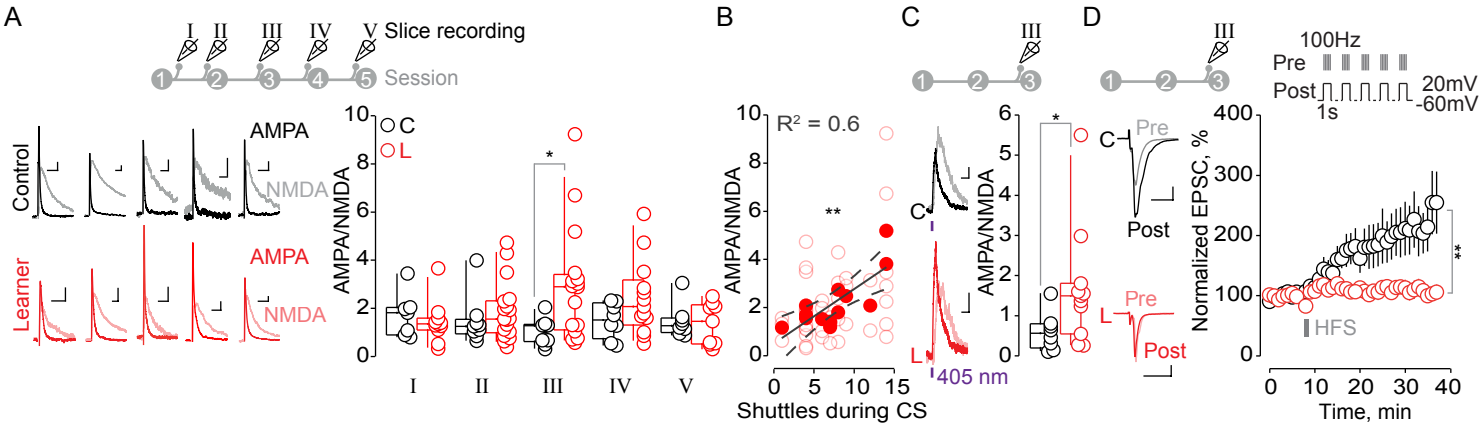

Trusel et al., Figure 2

Figure 3

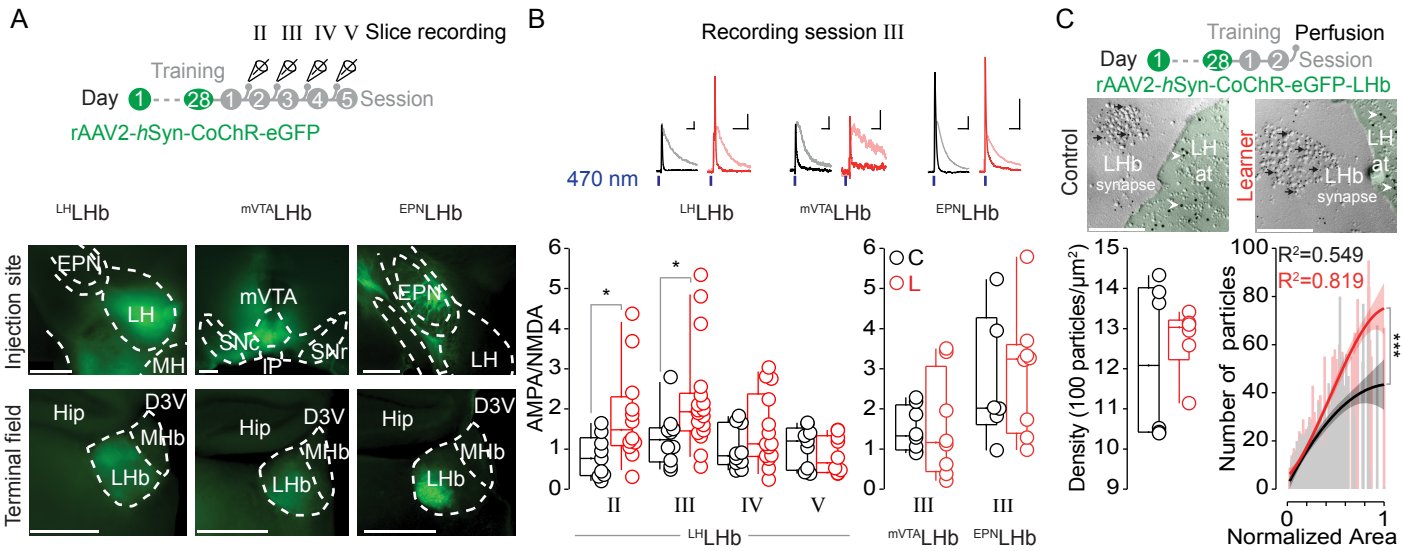

Trusel et al., Figure 3

Figure 4

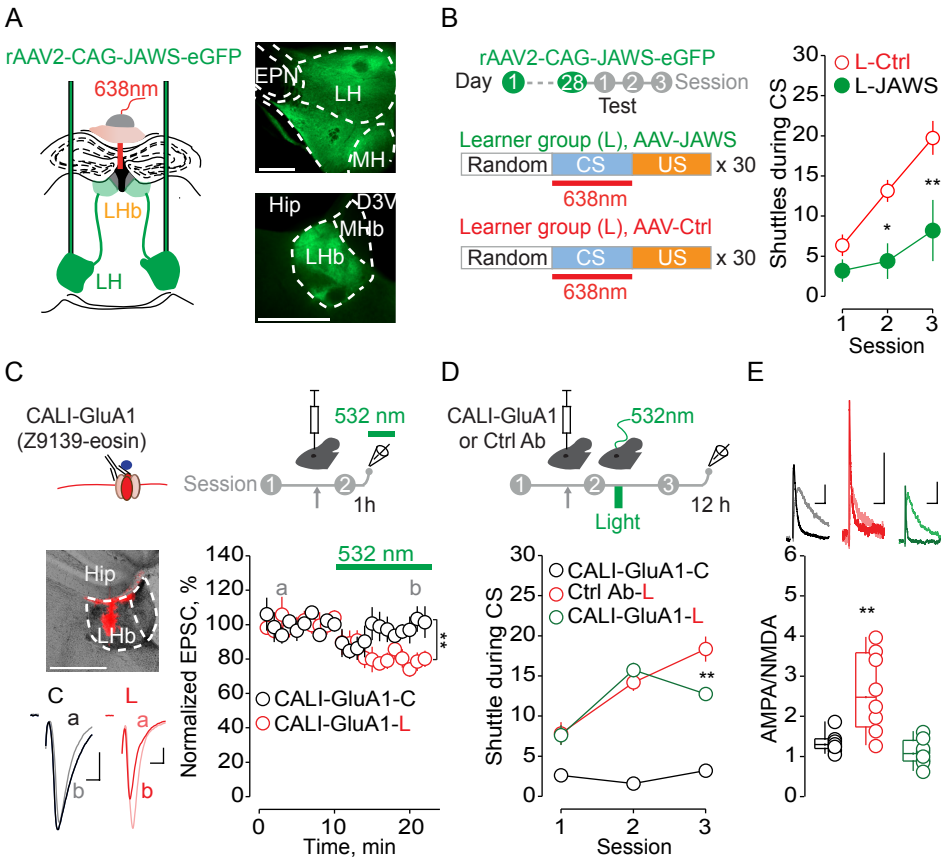

Trusel et al., Figure 4

Supplemental figure legends

Figure S1 Analysis of GCaMP6f signal in the LHb. Related to Figure 1

(A) Schematic representation of the two-way active avoidance behavioral test. Two identical compartments are separated by two walls, leaving a passage for the mouse to cross. After the CS onset, the mouse can stop the delivery of the footshock (through the electrified floor) by crossing the walls and reaching the opposite compartment.

(B) Schematic of a LHb-containing coronal section including the approximate sites of fibers placement (red circles, N=9).

(C) Representative image and magnification of GCaMP6f (green) and NeuN staining (red) in the LHb (scalebar: main=200μm, inset=50 μm). Plot reporting the total number of NeuN positive (outer circle, red) and the cells exhibiting GCaMP6f co-staining (inner circle, green) in 4 mice (black numbers, 3 LHb slices/mouse).

(D) Representative images (scalebar 250μm) and magnification (scalebar 20μm) of LHb slices displaying GCaMP6f expression (green), co-stained with the glutamatergic marker EAAC1 (red) and the GABAergic marker GAD67 (blue) in 2 different representative mice (scalebar: main=250μm, inset=20 μm). White arrowheads point to GCaMP6f neurons visibly co-stained with EAAC1, but not GAD67.

(E) Sample traces, box and scatter plot reporting the unchanged photon number measured across all sessions in control-trained mice infused with rAAV2.5-hSyn-GCaMP6f in LHb upon the delivery of the CS (N=5, RM One-way ANOVA Dunnett's D1 vs D5 $q_{4=}0.95$ $p>0.05$) and US (N=5, RM One-way ANOVA Dunnett's D1 vs D5 $q_{4=}0.87$ $p>0.05$).

(F) Sample traces, box and scatter plot reporting the unchanged photon number measured across all sessions in learner mice infused with rAAV2.5-hSyn-eGFP in LHb upon the delivery of the CS (N=5, RM One-way ANOVA

Dunnett's D1 vs D5 q_4=0.17 p>0.05) and US (N=5, RM One-way ANOVA Dunnett's D1 vs D5 q_4=0.96 p>0.05).

(G) Box and scatter plot reporting the unchanged normalized photon number measured across all sessions upon the delivery of US in Learner mice (US, N=9,RM One-way ANOVA Dunnett's D1 vs D5 $q_{8=}$0.49 p>0.05).

(H) Box and scatter plot reporting the unchanged photon number measured in naïve mice only exposed to 5 US at day 1 and 5 (N=4, average of 5 trials/mouse/day; t-test t_6=0.8 p>0.05).
Data are represented with box plots (median and quartiles).

(I) Normalized CS plotted in function of the photon noise at baseline for the learner group (correlation value/mouse; Spearman r=0.362, p>0.05, R^2 represents the goodness of fit).

(J) Timeline of awake head-fixed in vivo recordings, recording site (scalebar 1mm) and representative action potential (scalebar 0.2mV, 5ms). Raster plot (3 trials) and PSTH (10 trials) from a sample recording in a control and a learner mouse. Averaged z-score for all recordings in controls and learner mice (Controls: $n_{cells}/_{animals}$=41/2 vs Learners: $n_{cells}/_{animals}$=50/4; RM Two-way ANOVA, Controls vs Learners, $F_{1,73}$=2.63, p=0.02). Pie charts representing the distribution of CS-excited, CS-non responding and CS-inhibited neurons (Controls: CS_{Exc}=3, CS_{NR}=28, CS_{Inh}=10; Learners: CS_{Exc}=15, CS_{NR}=29, CS_{Inh}=6; X^2 t_2=8.2, p=0.02). Related scatter plot of the modulation index representing deviation of differential CS responses from zero (Arbitrary cutoff set at ±0.1).

Figure S2 Properties of excitatory transmission and synaptic plasticity within the LHb. Related to Figure 2 and Figure 3

(A) Correlation plot of AMPAR and NMDAR absolute current amplitudes evoked by MNI-Glutamate uncaging (NMDAR: controls 100.3±23.8, learners 80.6±18.9, t-test, t_{17}=0.6547 p>0.05; AMPAR: controls 38.5±5.8, learners

74.8±13.7, t-test, t_{17}=2.148 *p=0.0464; controls (C, black) $n_{cells}/_{animals}$=8/2; learners (L, red) $n_{cells}/_{animals}$=11/3).

(B) Sample traces and plot reporting the amplitude of trains (10 consecutive 20Hz pulses) of electrically-evoked EPSCs, normalized to the first EPSC (Two-Way Anova, $F_{1,22}$=0.67, p>0.05; controls (C, black) $n_{cells}/_{animals}$=12/7; learners (L, red) $n_{cells}/_{animals}$=12/7).

(C) Amplitude versus time plot of normalized EPSCs, and sample traces (50 pA, 10 ms) of EPSCs before (light line) and after (dark line) the conditioning protocol (HFS) in LHb-containing slices from naïve animals in presence or absence of the NMDAR antagonist APV (average $EPSC_{34\text{-}36\ min}$: naïve (blue), 154±11.8, $n_{cells/animals}$=6/4; +APV (green), 94.9±7.9, $n_{cells/animals}$=6/3; t-test, $t_{10=}$4.165 **p=0.0019).

(D) Box- and scatter plot reporting the maximal optically-induced current recorded during the optogenetic *ex-vivo* experiments with CoChR. Connectivity rate from subset of recordings: $n_{cellsEPSC}/n_{total}$, LH-LHb 50/50, EPN-LHb 18/18, mVTA 27/34.

(E) Experimental timeline and sample traces (20 pA, 20 ms) representing the AMPAR and NMDAR currents (+40 mV). Box and scatter plot of the AMPAR/NMDAR ratios 24 hours after session 4 at mVTA and EPN inputs (V, mVTA: controls (C, black) 0.9±0.2, $n_{cells}/_{animals}$=6/2; learners (L, red) 0.8±0.42, $n_{cells}/_{animals}$=6/2; t-test, $t_{10=}$0.4 p>0.05.V, EPN: controls (C, black) 3.1±0.9, $n_{cells}/_{animals}$=11/2; learners (L, red) 2.5±0.8, $n_{cells}/_{animals}$=11/2; t-test, $t_{20=}$0.46 p>0.05.).

(F) Experimental timeline and sample traces (20 pA, 20 ms) representing the AMPAR and NMDAR currents (+40 mV). Box and scatter plot of the AMPAR/NMDAR ratios at LH inputs 24 hours after a fear conditioning session (controls (gray) 1.4±0.3, $n_{cells}/_{animals}$=7/3; conditioned (green) 1.1±0.2; t-test, $t_{21=}$0.7 p>0.05).

(G) Amplitude versus time plot of normalized EPSCs, and sample traces (50 pA, 20 ms) of light-evoked EPSCs before (light line) and after (dark line) the LTP protocol (HFS) in LHb-containing slices from animals expressing the opsins CoChR and Chrimson in the LH (CoChR; average $EPSC_{34\text{-}36min}$: controls (C, black), 186.2±25.9, $n_{cells/animals}$=9/6; learners (L, red), 116.4±12.3, $n_{cells/animals}$=9/4; t-test, $t_{16=}$2.297 *p=0.0355. Chrimson; average $EPSC_{34\text{-}36min}$: controls (C, black), 225.2±26.3, $n_{cells/animals}$=6/2; learners (L, red), 113.5±17.3, $n_{cells/animals}$=3/2; t-test, $t_{7=}$2.8 *p=0.03). Data are represented as mean±SEM.

(H) Amplitude versus time plot of normalized EPSCs, and sample traces (100 pA, 20 ms) of light-evoked EPSCs before (light line) and after (dark line) the LTP protocol (HFS) in LHb-containing slices from animals expressing the opsins CoChR in the EPN (controls (C, black), average $baseline_{2\text{-}7min}$: 102.2±1.6, average $EPSC_{34\text{-}36min}$: 106.3±10.62, $n_{cells/animals}$=7/2; t-test, $t_{12=}$0.38 p>0.05).

(I) Amplitude versus time plot of normalized EPSCs, and sample traces (50 pA, 20 ms) of light-evoked AMPAR (-60 mV) and AMPAR+NMDAR (+40 mV) EPSCs before (a) and after (b) the LTP protocol (HFS) in LHb-containing slices from animals expressing the opsin CoChR in the LH (naive (black), average $baseline_{1\text{-}4min}$: 102.9±0.6, average $EPSC_{10\text{-}15min}$: 205.4±31.86, $n_{cells/animals}$=5/2; t-test, $t_{8=}$3.2 p=0.01). Box plot and scatter plot for AMPAR/NMDAR ratios before (a) and after (b) LTP together with a correlation plot between EPSC amplitude and AMPAR/NMDAR ratio (pre:1.8±0.4, post: 3.0±1.3, $n_{cells}/_{animals}$=5/2; Pre vs post paired t-test, $t_{6=}$3.0 *p=0.02.
Scatter plot and correlation analysis for fold-change of I_{AMPA} (post/pre- HFS), and the fold-change of the AMPAR/NMDAR (post/pre-HFS) (n=5, Pearson r=0.986, p=0.002, R^2 represents the goodness of fit).

Figure S3 Validation of silencing and inactivation tools in the LHb. Related to Figure 4

(A) Experimental timeline and sample image depicting JAWS-expressing fibers from LH in the LHb (green) and NeuN staining (red) (scalebar, main, 200 µm, inset, 20 µm). Amplitude versus time plot of normalized EPSCs

evoked by extracellular stimulation in the LHb in mice expressing the inhibitory opsin JAWS in the LH, and sample traces (100 pA, 20 ms), before (a, black) and after (b, red) the 584 nm light application (a: 99.5±0.3, b: 71.3±1.5, $n_{cells/animals}$=4/1, paired t-test, $t_{3=}$9.978 **p=0.0021).

(B) Peristimulus time histogram (PSTH) for footshock-evoked excitation (Fs, 0.5 s, 3mA, ISI: 5 s) reporting average spike counting for Fs-excited LHb neurons before and during exposure to 638 nm light in animals infused with rAAV2-CAG-JAWS-eGFP (Top) or rAAV2-hSyn-eGFP (Bottom). Box plots graph and scatter plot for shock-driven activity without/with light delivery (rAAV2-CAG-JAWS-eGFP: laser off (black) 10.3±0.9, laser ON (red) 4.2±1.2, $n_{cells}/_{animals}$=6/3; t-test, $t_{5=}$3.96 *p=0.01. rAAV2-hSyn-eGFP: laser off (black) 7.7±1.1, laser ON (red) 7.6±1.1, $n_{cells}/_{animals}$=4/2; t-test, $t_{3=}$0.037 p>0.05). Box plots referring to averaged firing activity during 1 second prior light ON (a), during light (b) and immediately after light off (rAAV2-CAG-JAWS-eGFP: laser off (a, black) 96.3±5.5, laser ON (b, red) 106.8±10.7, laser off (c, black) 100.2±7.1 $n_{cells}/_{animals}$=20/3; Friedman test, p>0.05. rAAV2-hSyn-eGFP: laser off (a, gray) 107.8±4.9, laser ON (b, pink) 101.6±1.5, laser off (c, gray) 102.5±4.0 $n_{cells}/_{animals}$=10/2; Friedman test, p>0.05).
Data are represented with box plots (median and quartiles).

(C) Schematic of a LHb-containing coronal section including the approximate sites of fibers placement (red circles, N=5) for in vivo JAWS experiments.

(D) Schematic of a LHb-containing coronal section including the approximate sites of fibers placement relative to the CALI in-vivo experiment (black circles, N=8, CALI-GluA1-C, green circles, N=8, CALI-GluA1-L).
Data are represented by mean±SEM.

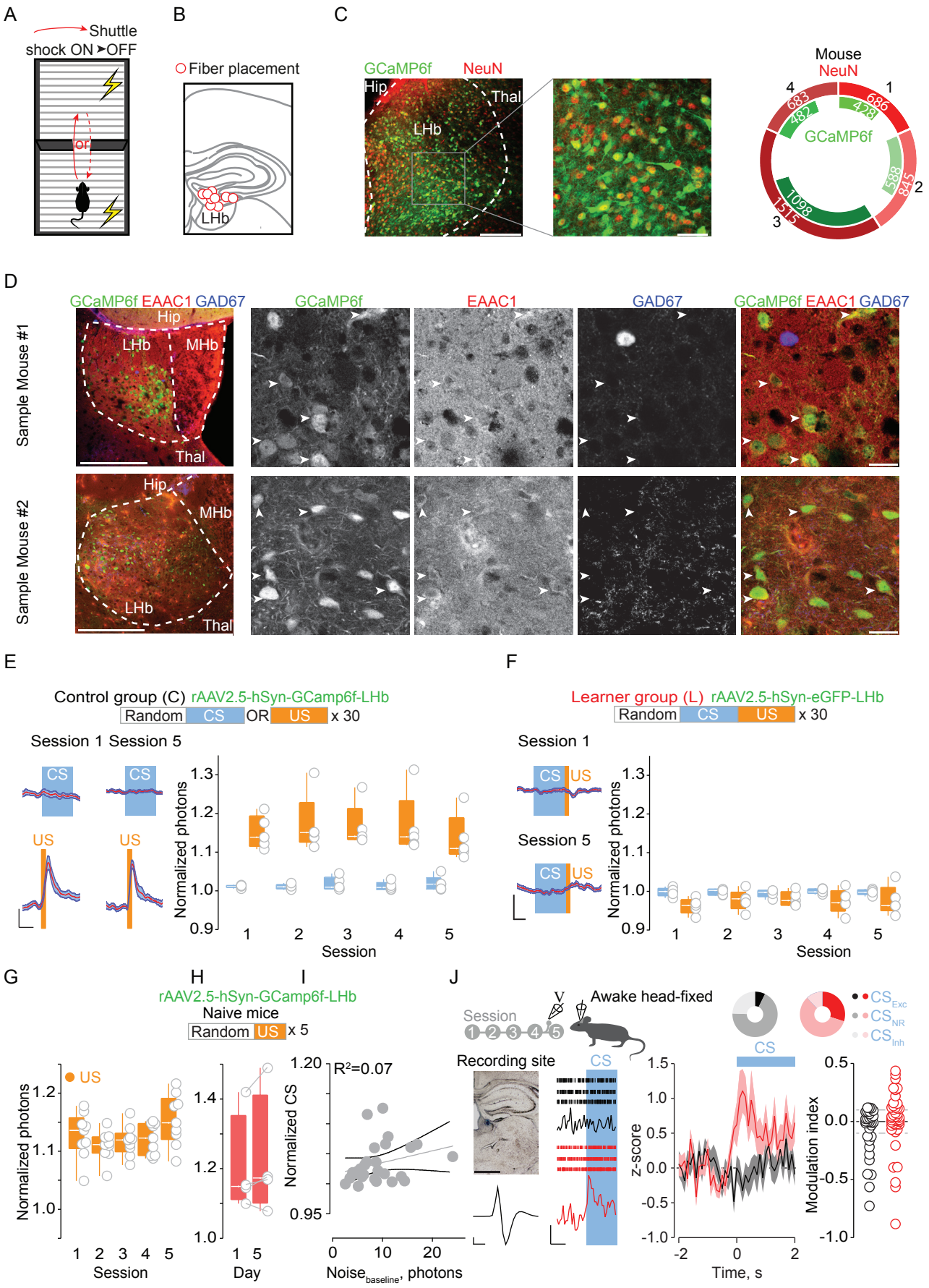

Trusel et al., Figure S1

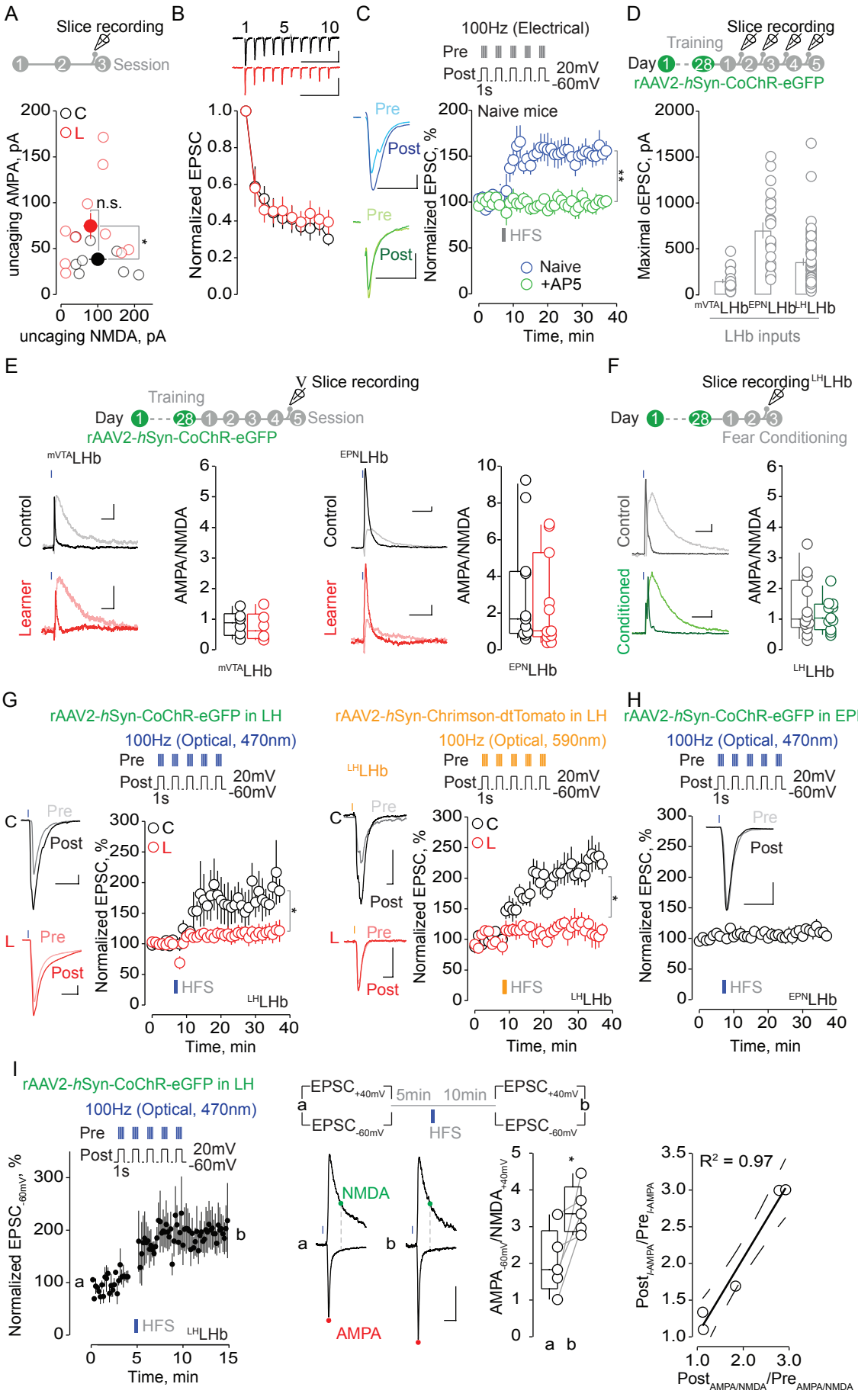

Trusel et al., Figure S2

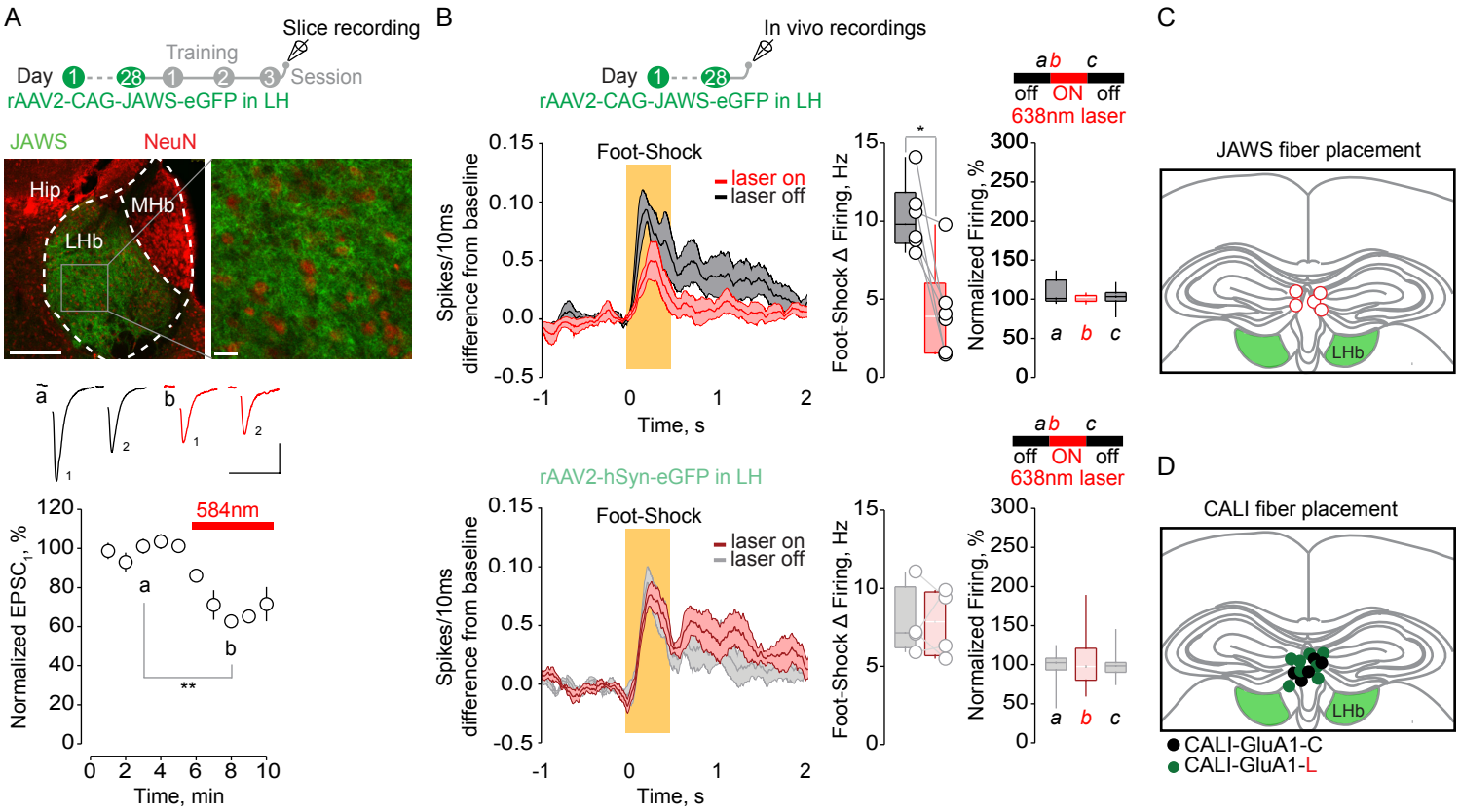

Trusel et al., Figure S3